Earth and Planetary Science Letters 525 (2019) 115751

Contents lists available at ScienceDirect

Earth and Planetary Science Letters

www.elsevier.com/locate/epsl

Barium in deep-sea bamboo corals: Phase associations, barium stable isotopes, & prospects for paleoceanography

Ben M. Geyman [a,b,c,1,2], Jamie L. Ptacek [c,2], Michèle LaVigne [c,*], Tristan J. Horner [a,b,*]

[a] NIRVANA Labs, Woods Hole Oceanographic Institution, Woods Hole, MA 02543, USA
[b] Department of Marine Chemistry & Geochemistry, Woods Hole Oceanographic Institution, Woods Hole, MA 02543, USA
[c] Department of Earth and Oceanographic Science, Bowdoin College, Brunswick, ME 04011, USA

ARTICLE INFO

Article history:
Received 18 May 2019
Received in revised form 28 July 2019
Accepted 30 July 2019
Available online xxxx
Editor: L. Robinson

Keywords:
GEOTRACES
isotope fractionation
northeast Pacific
paleoceanography
calcite
MC-ICP-MS

ABSTRACT

Reconstruction of past seawater $\delta^{138/134}Ba_{NIST}$ (barium-isotopic compositions) can augment existing proxies of water mass provenance and deep-ocean circulation. Deep-sea bamboo corals are uniquely poised to record Ba-isotopic variations, given their widespread oceanographic distribution and incorporation of ambient Ba in approximate proportion to that in surrounding seawater. However, the utility of such records requires knowing: the phases hosting Ba in deep-sea coral skeletons, that specimens faithfully capture modern Ba-isotopic chemistry, and that internal skeletal variability relates principally to historical variations in the composition of ambient seawater. We investigated each of these requirements using a stepped cleaning experiment, a 'core-top' comparison of eight live-collected specimens from the California margin (870–2,055 m) against ambient seawater, and through examination of historical variability in skeletal Ba chemistry, respectively. First, we report that non-carbonate phases minimally contribute to bamboo coral Ba/Ca, obviating the need for chemical cleaning of live-collected specimens. Second, using newly-obtained profiles of northeast Pacific Ba-isotopic chemistry, we observe that bamboo corals faithfully reflect ambient seawater with a taxonomically- and environmentally-invariant Ba-isotopic offset, $\Delta^{138/134}Ba_{coral-SW}$, of $-0.37\pm0.03‰$ (±2 SD, $n = 8$). The partition coefficient for Ba, K_D^{Ba}, is similarly insensitive to taxonomy, but linearly decreases with depth. The driving mechanism is unresolved. Third, we find minimal Ba/Ca and Ba-isotopic variability in historical growth representing the past century. We interpret this invariance as evidencing the overall fidelity of deep-sea bamboo corals for ambient Ba chemistry over their long lifespans. The insensitivity of $\Delta^{138/134}Ba_{coral-SW}$ to environmental gradients indicates that the Ba-isotopic composition of bamboo corals can be solely interpreted in terms of seawater composition, which should find myriad applications to the study of past ocean circulation over a range of timescales.

1. Introduction

The voluminous intermediate- and deep-ocean store climatically-important quantities of heat, carbon, and nutrients. Ventilation of these deep waters is essential for returning nutrients to the main thermocline, and thus the overturning circulation plays a major role in modulating Earth's climate on decadal to millennial timescales (e.g., Toggweiler, 1999; Sigman et al., 2010). However, almost all knowledge of ocean circulation prior to modern observations is necessarily derived from geochemical or other proxy records (e.g., Thresher et al., 2004; Adkins, 2013). Of the marine 'record keepers', deep-sea bamboo corals have emerged as particularly powerful biogeochemical archives since these corals are long-lived, are both vertically and geographically widespread within the ocean interior (between 400–3,000 m and found in all major ocean basins), and are amenable to radiocarbon dating (e.g., Hill et al., 2014; Farmer et al., 2015; Frenkel et al., 2017). The composition of the high-Mg calcitic internodes of deep-sea bamboo corals is known to correlate with certain properties of ambient seawater, such as temperature and nutrient content (e.g., Thresher et al., 2010; LaVigne et al., 2011; Sinclair et al., 2011; Saenger and Watkins, 2016; Prouty et al., 2017). Further, the chemistry of their gorgonin nodes—proteinaceous ligaments derived

* Corresponding authors.
E-mail addresses: mlavign@bowdoin.edu (M. LaVigne), Tristan.Horner@whoi.edu (T.J. Horner).
[1] Now at: School of Engineering and Applied Science, Harvard University, Cambridge, MA 02138, USA.
[2] These authors contributed equally to this work.

https://doi.org/10.1016/j.epsl.2019.115751
0012-821X/

from sinking particulate matter (Roark et al., 2005; Sherwood and Risk, 2007)—provide a contemporaneous window into local surface processes, such as productivity and remineralization (e.g., Hill et al., 2014).

Of the various nutrient tracers in bamboo corals, Ba (barium) is one of the most promising; dissolved Ba concentrations (henceforth $[Ba]_{SW}$) closely follow those of other algal nutrients (notably Si, as silicic acid; Wolgemuth and Broecker, 1970), and the Ba/Ca ratio of the calcitic internodes exhibits a linear relationship to ambient Ba concentrations (LaVigne et al., 2011; Thresher et al., 2016). The underlying driver of marine Ba cycling is likely related to the mineral $BaSO_4$ (barite). Discrete, micron-sized crystals of $BaSO_4$ are a ubiquitous component of marine particulate matter (e.g., Dehairs et al., 1980; Bishop, 1988). These crystals are thought to form in association with the microbial oxidation of organic matter in the upper mesopelagic (200–1,000 m; e.g., Chow and Goldberg, 1960). This process renders a significant negative Ba-isotopic fractionation whereby isotopically-light Ba is incorporated into $BaSO_4$ (von Allmen et al., 2010), and residual, Ba-depleted seawater is correspondingly enriched in isotopically-heavy Ba (Horner et al., 2015). Isotopic profiles of dissolved Ba in seawater reflect this general pattern, albeit with a strong modulation by the meridional overturning circulation (e.g., Bates et al., 2017; Hsieh and Henderson, 2017). Indeed, in the Atlantic Ocean, recent results revealed that Ba distributions below the mesopelagic are almost entirely controlled by conservative mixing of water masses with distinct Ba-isotopic compositions (Bates et al., 2017). It thus follows that depth-resolved records of Ba-isotopic compositions will offer a powerful window into the circulation of water masses in the intermediate- and deep-ocean in Earth's past.

In addition to being a powerful tracer of ocean chemistry, Ba is well-preserved in bamboo corals. The high-Mg calcitic internodes of several species of deep-sea bamboo coral are known to exhibit a linear dependence between skeletal and ambient Ba/Ca, with a slope above unity (e.g., LaVigne et al., 2011; Thresher et al., 2016; Flöter et al., 2019). This raises three important issues. First, bamboo corals are unusual in that, despite precipitating calcite, they exhibit Ba/Ca ratios in excess of ambient seawater. In contrast, calcites precipitated inorganically (e.g., Mavromatis et al., 2018), found in core-top sediments (e.g., Lea and Boyle, 1989), or grown in culture (e.g., Lea and Spero, 1994; Hintz et al., 2006) generally exhibit lower-than-ambient Ba/Ca. This enrichment could derive from calcification itself, or could reflect incorporation of other Ba-rich particulate phases. Such phases could include organic matter—the principal food source to bamboo corals—or physically encased detritus or micro-crystalline $BaSO_4$, which are particularly abundant in the meso- and bathypelagic ocean (up to 10^4 crystals per L; Dehairs et al., 1980). Second, while recent studies report that aragonitic corals are faithful archives of ambient Ba-isotopic chemistry (Hemsing et al., 2018; Liu et al., 2019), there is no equivalent calibration for calcitic deep-sea corals. Moreover, there are no Ba-isotopic calibration data for any species of deep-sea coral from the nutrient-rich and $[O_2]$-poor Pacific Ocean. Third, it is not known whether deep-sea bamboo corals are reliable recorders of ambient barium chemistry over their entire life history, which can span several hundred years (e.g., Thresher et al., 2004; Sherwood and Edinger, 2009; Flöter et al., 2019). Addressing these three issues could improve confidence in barium-based bamboo coral paleoceanographic reconstructions and add a powerful new proxy to the expanding list of paleoenvironmental properties captured by these long-lived archives.

Here, we address all three of these issues by presenting a systematic assessment of the utility of Ba in deep-sea bamboo corals from the Pacific Ocean. This assessment has three complementary components: First, we established the most likely mechanism of Ba incorporation into the calcitic internodes of bamboo corals by performing a stepped-cleaning experiment designed to test for any non-lattice bound Ba in organic matter and encased $BaSO_4$. Second, we investigate the fidelity of bamboo corals to record ambient Ba-isotopic chemistry by analyzing 24 modern samples from eight northeast Pacific coral specimens. To facilitate this calibration, we report the first high-resolution, full-ocean depth profile of Ba-isotopic compositions from the Pacific Ocean at 'SAFe' (30 N, 140 W). Third, we examined temporal trends in skeletal Ba chemistry by analyzing historical growth bands from six of the eight specimens used in the modern calibration. Assuming that our results from the northeast Pacific can be extended to deep-sea bamboo corals from other ocean basins, our results indicate that the Ba-isotopic compositions of fossil carbonates should find utility in studying patterns of past ocean circulation over a range of timescales.

2. Samples, sampling, and methods

2.1. Samples

2.1.1. Deep-sea corals

Corals were collected from the Pioneer, San Juan, and Davidson Seamounts, and from Monterey Canyon in 2004 and 2007 using the ROV *Tiburon*, deployed from the R/V *Western Flyer*. Coral skeletons were cleaned of organic tissue, rinsed, and air dried before archiving at the University of California, Davis. Specimens were identified based on morphological characteristics as belonging to the *Isidella* and *Keratoisis* subfamilies (Table 1), though other related taxa may be represented (e.g., France, 2007; LaVigne et al., 2011; Hill et al., 2014). Chronologies were established for six corals based on the location of the radiocarbon 'bomb spike' using the non-linear growth model presented by Frenkel et al. (2017; Sec. 2.3; Supplement).

2.1.2. Seawater

Profiles of dissolved [Ba] and Ba-isotopic compositions were determined using samples collected at two locations in the northeast Pacific. During both cruises, seawater samples were handled using metal-clean GEOTRACES protocols (e.g., Cutter et al., 2010). Samples from the first site, SAFe (30 N, 140 W; Table 1), were collected in May 2009 aboard the R/V *Knorr* during the second GEOTRACES intercalibration cruise (KN195-08). A full profile (1–4,500 m) was constructed using samples from the filter test experiments. These samples were filtered to 0.2 or 0.4 µm using either Osmonics, Pall Acropak, or Satrobran acid-cleaned filter cartridges; a systematic comparison of the different filter types was conducted to assess whether filter cutoff had any effect on measured Ba chemistry (see Supplement). Samples from the second site, close to the California Margin (39 N, 126 W; Fig. 1), were collected and filtered to 0.4 µm in July 2014 aboard the R/V *Melville* during 'IrnBru' (MV1405). A composite water column profile spanning depths 15–1,500 m was constructed using samples from St. 12 (15–95 m) and St. 12b (118–1,500 m), collected at approximately the same location on 2014-07-11 and 2014-07-13, respectively. Dissolved $[Ba]_{SW}$ data from IrnBru were reported in Serrato Marks et al. (2017).

2.2. Sampling

2.2.1. Corals

Recent growth was sampled from the basal internodes of eight specimens, hereafter termed 'modern edge' samples (Table 1). Fresh cross-sections were cut using a rotary tool (Dremel 400 series, Dremel, Wisconsin USA), cleaned via sonication in 0.2 M HNO_3, thrice rinsed with 18.2 MΩ·cm-grade H_2O (Milli-Q, MilliporeSigma, Massachusetts, USA), and air-dried. Three 15 mg samples of calcite powder were routed from distinct locations around

Table 1
Sample information. Collection details for seawater (upper) and bamboo corals (lower) analyzed in this study. All coral specimens, except for T1101 A14 and T664 A1, had living polyps present at the base of the colony at the time of collection. *Denotes specimen that was subsampled for historical interior Ba/Ca and Ba-isotopic analysis.

Site	Deployment	Latitude (°N)	Longitude (°W)	Sample #	Year collected	Depth (m)
SAFe	KN195-08	30	140	Seawater profile	2009	1–4,500
California Margin	MV1405	39	125.75	Seawater profile	2014	15–1,500
Monterey Canyon	T1104	36.74	122.03	A7* (*Isidella*)	2007	870
Pioneer Seamount	T1101	37.37	123.40	A5 (*Keratoisis*)	2007	1,004
				A7* (*Isidella*)		1,005
		37.37	123.41	A14 (*Isidella*)		1,010
				A10* (*Isidella*)		1,092
Davidson Seamount	T1102	35.73	122.73	A12* (*Keratoisis*)	2007	1,500
				A10* (*Keratoisis*)		1,521
San Juan Seamount	T664	33.15	120.89	A1* (*Isidella*)	2004	2,055

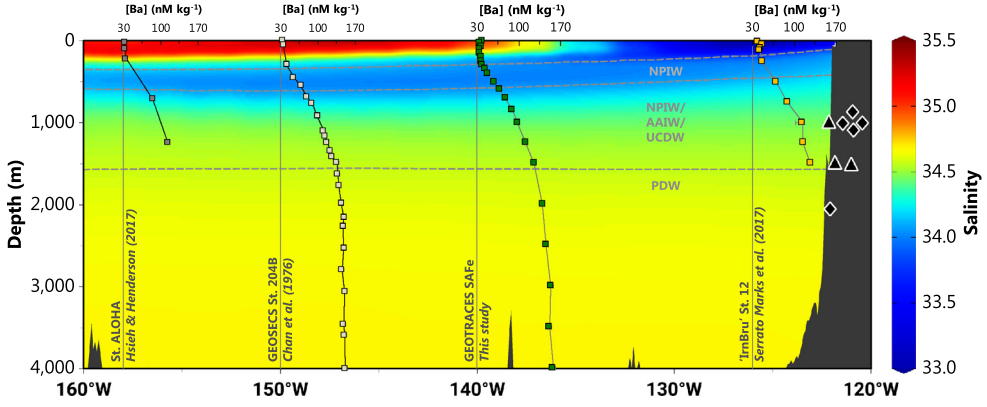

Fig. 1. North Pacific hydrography. Section of salinity from St. ALOHA (22 °N, 158 °W; on left) to the California Margin (St. 12b of IrnBru, 39 °N, 126W) through GEOSECS St. 204 (31 °N, 150 °W; Chan et al., 1976) and SAFe (30 °N, 140 °W). Profiles of dissolved $[Ba]_{SW}$ are shown at each station, with the sampling longitude marked by the solid vertical line. Diamonds (*Isidella*) and triangles (*Keratoisis*) along the California Margin denote the depths corresponding to the deep-sea bamboo corals used in this study; symbols have been horizontally spaced for clarity (exact coordinates given in Table 1). Dashed lines indicate isopycnal surfaces corresponding to $\sigma_\theta = 26.2$ (shallowest), 26.9, and 27.6 kg m^{-3} (deepest). Water masses have been identified based on their density as per Talley (2008): NPIW (North Pacific Intermediate Water), AAIW (Antarctic Intermediate Water), UCDW (Upper Circumpolar Deep Water), and PDW (Pacific Deep Water). Salinity data from World Ocean Database (Boyer et al., 2018).

the outer 2 mm of each internode using a 0.3 mm diameter diamond-tipped rotary scriber, yielding 24 samples of most recently precipitated calcite. Resultant powders were stored dry until chemical cleaning (Sec. 2.2.2).

Six of the eight specimens used for the modern edge calibration were further subsampled to assess historical patterns in Ba chemistry, henceforth termed 'historical interior' samples. Fresh faces were cut using a rock saw, rinsed using 18.2 MΩ·cm-grade H_2O, air dried, and mounted to a glass slide using cyanoacrylate adhesive. Concentric circular troughs were micromilled from each face using a 0.8 mm diameter carbide scriber and carefully following visible growth bands by (New Wave; ESI, Omaha, Nebraska, USA). Between three and five historical interior samples were milled from of six specimens (Table 1), yielding 24 historical interior samples. A scaling method, based on that described for alignment of individual laser ablation tracks (Serrato Marks et al., 2017), was used to account for any unevenness in the banding. Based on cleaning experiment results (Sec. 3.2.1), cleaning of historical interior sample powders was deemed unnecessary.

2.2.2. Cleaning experiments

Phase associations were investigated by documenting changes in skeletal Ba/Ca through each step of a sequential cleaning experiment, performed in laminar flow clean benches at Bowdoin College. The results of these tests were validated using high-resolution imaging via scanning electron microscopy (SEM; see Supplement). These experiments tested for the presence of any non lattice-bound Ba, such as that present in inter-crystalline organic matter or $BaSO_4$, using an oxidizing agent (H_2O_2, hydrogen peroxide) and alkaline pentetic acid (DTPA; see e.g., Lea and Boyle, 1993), respectively. (Note that corals were collected live and did not possess Fe-Mn coatings, rendering reductive cleaning unnecessary.) A detailed cleaning protocol is provided in Table S1. Briefly, 3 mg of powder was isolated from each of the modern edge samples. From this, 1 mg was used to test each cleaning treatment: no treatment, oxidative only, and oxidative-followed-by alkaline DTPA. After treatment, powder samples were rinsed with 18.2 MΩ·cm-grade H_2O and air dried. The remaining ≈12 mg of modern edge material were subjected to the full cleaning treatment prior to Ba/Ca and Ba-isotopic analysis.

2.3. Analytical methods

Sample handling took place within class 100 laminar flow workstations at the NIRVANA clean labs (Non-traditional Isotope Research on Various Advanced Novel Applications), at WHOI (Woods Hole Oceanographic Institution). Labware was acid-cleaned prior to use and samples manipulated using only ultra-pure, in-house double-distilled reagents.

Coral powders were submerged in 18.2 MΩ·cm-grade H_2O, dissolved via dropwise addition of 6 M HCl, dried, and reconstituted in 2 mL of 2 M HCl. Aliquots of this solution were analyzed for [Ba] and Ba/Ca using quadrupole ICP-MS (iCAP Q, Thermo Fisher Scientific, Massachusetts, USA) at the WHOI Plasma Facility. Quantification was achieved by comparison of indium- and blank-corrected ion beam intensities between samples and a serially-diluted reference standard containing known concentrations of Ba and Ca. Subsequently, aliquots containing ∼50 ng of Ba were isolated and

a ^{135}Ba–^{136}Ba double spike added to achieve a spike:sample ratio between 1–2 (Bates et al., 2017). Samples were fluxed for ≥12 hours in a 1 mL mixture of concentrated HNO_3–H_2O_2 (to oxidize any recalcitrant organic matter), before conversion to Cl form via repeated addition and drying with concentrated HCl. Samples were reconstituted in 250 µL of 2 M HCl prior to ion-exchange chromatography.

Aliquots containing 5 mL of acidified seawater were appropriately spiked, de-salted via co-precipitation with $CaCO_3$ (Horner et al., 2015), and the resultant precipitate similarly dissolved in 250 µL of 2 M HCl for ion-exchange chromatography. Coral and seawater samples were twice passed through ion-exchange columns containing 500 µL of pre-cleaned Bio-Rad AG 50W-X8 cation-exchange resin; major elements were eluted in 2 M HCl and Ba eluted with 2 M HNO_3 (Horner et al., 2015). The final eluent was reconstituted in an appropriate volume of 2% HNO_3 to achieve a non-spike [Ba] of ≈20 ng/mL.

Barium-isotopic analyses were performed using a Thermo Finnigan Neptune multi-collector ICP-MS, also situated at the WHOI Plasma Facility. Detailed measurement protocols are described in Horner et al. (2015). All samples were analyzed a minimum of $n = 3$ times within a given analytical session, though samples containing larger quantities of Ba were typically analyzed many more times; median $n = 6$ and 7 for coral and seawater samples, respectively. Each Ba-isotopic analysis was weighted by the inverse square of its respective measurement uncertainty, and a weighted mean composition calculated relative to NIST SRM 3104a:

$$\delta^{138/134}\mathrm{Ba}_{\mathrm{NIST}}(‰) = (^{138}\mathrm{Ba}/^{134}\mathrm{Ba})_{\mathrm{sample}} / (^{138}\mathrm{Ba}/^{134}\mathrm{Ba})_{\mathrm{NIST\ SRM\ 3104a}} - 1 \quad (1)$$

Blanks were monitored by passing ng-sized aliquots of double spike through the relevant processing pipeline (i.e., corals or seawater) and Ba concentrations determined by isotopic dilution. (Coral Ba/Ca data were determined separately and not subject to processing blanks.) Coral processing blanks for $\delta^{138/134}\mathrm{Ba}_{\mathrm{NIST}}$ yielded a mean of 64±83 pg of Ba (±SD; $n = 6$). Seawater blanks were somewhat higher at 1.8±0.8 ng (±SD; $n = 4$), which likely resulted from co-precipitation, necessitating a minor blank correction to $[\mathrm{Ba}]_{\mathrm{SW}}$ data (≤7%). Since our blank possesses $\delta^{138/134}\mathrm{Ba}_{\mathrm{NIST}}$ ≈0‰ (Horner et al., 2015), no blank correction was applied to any Ba-isotopic data for either coral or seawater samples, which possessed ∼50 and between 25–100 ng Ba, respectively.

Long-term reproducibility is estimated as ±2.5% for $[\mathrm{Ba}]_{\mathrm{SW}}$, ±4.9% for Ba/Ca, and ±0.03‰ for $\delta^{138/134}\mathrm{Ba}_{\mathrm{NIST}}$. These uncertainties are based on repeat measurements of carbonate and seawater reference materials, discussed in the next section. All uncertainties reported as ±2 SD.

Age models were constructed for each of the six corals used for historical reconstructions of Ba/Ca and $\delta^{138/134}\mathrm{Ba}_{\mathrm{NIST}}$. These age models were based on ^{14}C (radiocarbon) ages using data published by Frenkel et al. (2017; for corals T1101 A7, T1101 A10, T1102 A12), Hill et al. (2014; for specimen T664 A1), and new ^{14}C data (*this study*; for T1104 A7 and T1102 A10). Samples were decalcified, cleaned, the gorgonin nodes peeled, and analyzed for Δ^{14}C at the National Ocean Sciences Accelerator Mass Spectrometry Facility, situated at WHOI following the approach described by Frenkel et al. (2017; Supplement).

3. Results

3.1. Northeast Pacific seawater

Accuracy of seawater measurements was assessed by processing GEOTRACES seawater reference materials from the northeast Pacific alongside samples. We find that SAFe S (surface seawater), SAFe D1 (1,000 m), and SAFe D2 (1,000 m) possess $[\mathrm{Ba}]_{\mathrm{SW}}$ and $\delta^{138/134}\mathrm{Ba}_{\mathrm{NIST}}$ of: 34.7±0.9 nmol/kg and +0.63±0.04‰, 98.7±2.5 nmol/kg and +0.31±0.03‰, and 97.2±2.4 nmol/kg and +0.32±0.03‰, respectively, which are in agreement with those reported for SAFe S (34.3 nmol/kg, +0.62±0.02‰) and D1 (99.6 nmol/kg, +0.27±0.02‰) by Hsieh and Henderson (2017).

At SAFe, dissolved $[\mathrm{Ba}]_{\mathrm{SW}}$ exhibits a characteristic nutrient-like profile, with a minimum at 25 m of 35.0±1.9 nmol/kg, which increases monotonically with depth, before reaching a deep, broad maximum of 157.6±3.2 nmol/kg at ≈4,000 m depth; dissolved $\delta^{138/134}\mathrm{Ba}_{\mathrm{NIST}}$ shows the opposite pattern, decreasing from +0.61±0.03‰ to +0.22±0.03‰. Our profile of $[\mathrm{Ba}]_{\mathrm{SW}}$ at SAFe is similar to that obtained at St. 204b of GEOSECS, collected in 1973 (31 N, 150 W; Chan et al, 1976; Figs. 1 & 2). Dissolved Ba*, the difference between measured and 'expected' $[\mathrm{Ba}]_{\mathrm{SW}}$ (Bates et al., 2017), exhibits a profile similar to that of dissolved $[O_2]$, with a minimum approaching −25 nmol/kg between 700−1,000 m (Fig. 2).

Data from the California Margin also show systematic, depth-dependent increases in $[\mathrm{Ba}]_{\mathrm{SW}}$ from 39.9±2.5 to 127.2±3.5 nmol/kg and decreases in $\delta^{138/134}\mathrm{Ba}_{\mathrm{NIST}}$ from +0.52±0.05‰ to +0.30±0.03‰ over the length of the profile (15–1,500 m). These patterns are similar to SAFe, albeit with two notable differences. First, the maximum in $\delta^{138/134}\mathrm{Ba}_{\mathrm{NIST}}$ is not observed at the very surface, but instead occurs below the euphotic zone, similar to profile data from the subtropical North Atlantic (Bates et al., 2017). Second, all Ba-related properties exhibit steeper gradients close to the California Margin, concomitant with a marginward shoaling of isopycnal surfaces (Figs. 1 & 2). When plotted in property–property space however, all data from the northeast Pacific collapse onto a single mixing trend similar to that reported from other ocean basins (Fig. 3).

The margin sample from 1,000 m possesses an anomalously low spike-to-sample ratio (≈1.3) relative to neighboring profile samples (≈1.4), which translates into high implied $[\mathrm{Ba}]_{\mathrm{SW}}$ (and Ba*; Fig. 2). Oceanographically consistent [Si] and $\delta^{138/134}\mathrm{Ba}_{\mathrm{NIST}}$ rule out a potential bottle 'misfire' and the ion-exchange yields are similar to other profile samples, ruling out contamination. Thus, high $[\mathrm{Ba}]_{\mathrm{SW}}$ could reflect either a true hydrographic feature or evaporation. The former implies input from a source characterized by $\delta^{138/134}\mathrm{Ba}_{\mathrm{NIST}}$ ≈ +0.6‰, whereas the latter requires water loss from the small sample volumes retained for Ba-isotopic analysis (≤15 mL). Since we cannot discriminate between these scenarios, we report $[\mathrm{Ba}]_{\mathrm{SW}}$ 'as measured', but assign an asymmetric uncertainty to indicate the effect of evaporative losses, estimated from the spike-to-sample ratios of adjacent profile samples.

3.2. Deep-sea corals

Accuracy was monitored by processing JCp-1, a surface coral powder standard, alongside samples. We find that JCp-1 possesses Ba/Ca and $\delta^{138/134}\mathrm{Ba}_{\mathrm{NIST}}$ of 7.1±0.4 µmol/mol and +0.28±0.03‰, respectively. Both quantities agree with the inter-laboratory mean Ba/Ca of 7.5±1.3 µmol/mol (Hathorne et al., 2013) and published Ba-isotopic compositions, both from our lab (+0.29±0.03‰; Horner et al., 2015) and others; Hemsing et al. (2018) and Liu et al. (2019) report $\delta^{138/134}\mathrm{Ba}_{\mathrm{NIST}}$ = +0.25±0.03‰ and +0.30±0.03‰, respectively.

3.2.1. Phase associations

Neither of the cleaning treatments resulted in Ba/Ca changes exceeding either long-term measurement precision (±4.9% 2 RSD) or the ±2 SD variability in the effect itself (for $n = 8$ specimens; Table 2). Compared to untreated powders, oxidative cleaning

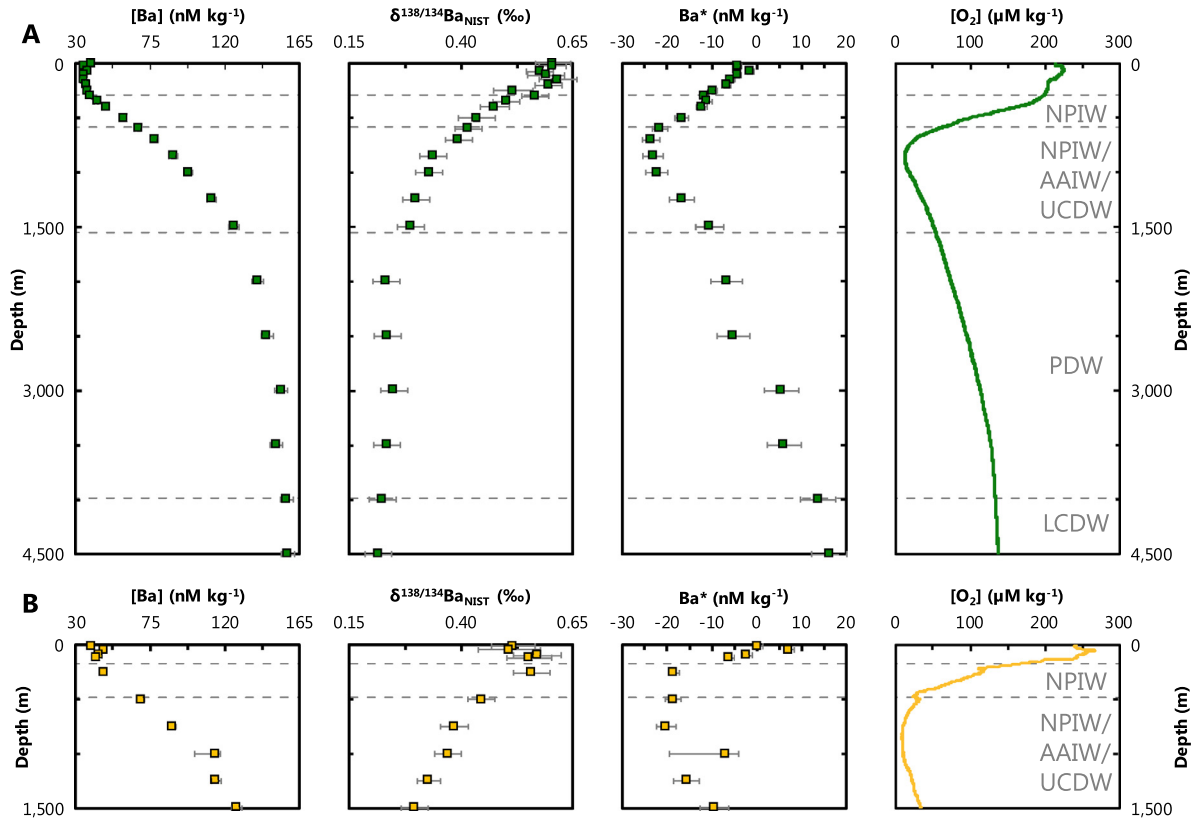

Fig. 2. Barium in the northeast Pacific. Property–depth plots at (A) SAFe and (B) St. 12b of 'IrnBru', close to the California Margin. From left–right: barium concentration, stable isotope composition, barium 'star', and dissolved oxygen. ($Ba^* = [Ba]_{SW} - [Si] \times 0.6296 - 38.63$; Bates et al., 2017.) Note the shallower occurence of intermediate waters, particularly NPIW, along the California Margin. Water mass designations and abbreviations as per Fig. 1; LCDW denotes Lower Circumpolar Deep Water. Evaporation is suspected for the sample collected at 1,000 m from the California Margin (see text).

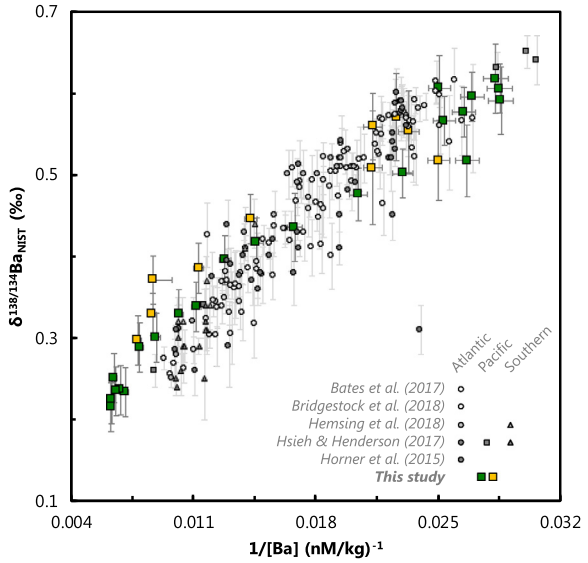

Fig. 3. Global correlation between dissolved Ba-isotopic compositions and the reciprocal of Ba concentration. Data from *this study* indicate that seawater from the northeast Pacific also fall along the array defined by samples from the Atlantic and Southern Oceans. Barium-replete samples from the core of PDW possess $\delta^{138/134}Ba_{NIST} \approx +0.2$‰, which are amongst the lightest yet reported for the open ocean. For clarity, uncertainties on 1/[Ba] have been omitted from literature data, but are generally similar to those reported here (±2.5%).

caused an average change in Ba/Ca of −1.4±2.8%, while oxidative-then-alkaline DTPA cleaning rendered a larger and more variable change of −4.0±4.1% (mean±2 SD). The large powder samples—for subsequent Ba-isotopic analysis—were subjected to the full oxidative-then-alkaline DTPA chemical cleaning procedure and exhibited a similarly negligible change in Ba/Ca of +1.2±4.4% relative to untreated powders.

The effect of reductive chemical cleaning on Ba/Ca was not investigated since all corals were collected live (i.e., absent Fe-Mn coatings). Reductive cleaning may be important for fossil specimens, however. As a baseline for future studies, we report Fe/Ca and Mn/Ca for the modern, untreated specimens as 13.3±1.6 and 0.8±0.5 μmol/mol, respectively (mean±SD, $n = 8$; Supplement).

Results from the SEM analyses revealed no evidence for encased $BaSO_4$ crystals in any of the coral samples analyzed. The lack of encased $BaSO_4$ was validated by examining coral powders using backscattered electron microscopy and energy-dispersive x-ray spectroscopy (Supplement).

3.2.2. *Spatiotemporal variations in skeletal Ba chemistry*

The eight specimens exhibit mean Ba/Ca and $\delta^{138/134}Ba_{NIST}$ spanning 12.8–15.2 μmol/mol and −0.12 to +0.01‰, respectively (Fig. 4). Excepting a single subsample from specimen T664 A1 that we suspect of contamination during micromilling, the six specimens analyzed for historical Ba chemistry yield similar ranges in Ba/Ca and $\delta^{138/134}Ba_{NIST}$, spanning 12.5–14.8 μmol/mol and −0.13 to +0.02‰, respectively (Fig. 5). Note that each modern edge Ba/Ca and Ba-isotopic measurement was obtained using ≈12 mg of residual powder, subject to the full cleaning procedure, that were dissolved separately to the 1 mg powders used in the cleaning experiments. Historical interior powders were not subject to chemical cleaning. All historical interior samples are within analytical uncertainty of their respective modern edge for both Ba/Ca and $\delta^{138/134}Ba_{NIST}$ (Fig. 5). Intra-specimen variability is significantly smaller than the inter-specimen ranges for both modern edges and historical interior samples. Intra-specimen

Table 2
Stepped chemical test results. Results for Ba/Ca are given as the (unweighted) mean of the triplicate measurements from each specimen. Uncertainties are reported as the greater of either ±2 SD of the triplicates or as long term precision. Relative to no treatment, oxidative and oxidative-then-DTPA treatment render mean effects of −1.4±2.8% and −4.0±4.1%, respectively (both reported as ±2 SD, $n = 8$). Neither effect is outside of long-term ±2 SD precision of ±4.9%, indicating that cleaning does not significantly alter skeletal Ba/Ca.

Specimen	No treatment		Oxidative treatment		Oxidative & DTPA treatment	
	Ba/Ca (μM/M)	±2 SD (μM/M)	Ba/Ca (μM/M)	±2 SD (μM/M)	Ba/Ca (μM/M)	±2 SD (μM/M)
T1104 A7	12.7	0.6	12.9	2.3	12.2	0.6
T1101 A5	13.2	0.7	13.1	1.0	12.6	1.0
T1101 A7	12.8	0.6	12.6	0.6	12.6	0.7
T1101 A14	12.3	0.6	12.2	0.6	12.2	1.1
T1101 A10	12.4	0.6	12.2	0.6	12.0	1.1
T1102 A12	15.3	0.8	14.7	0.7	14.3	0.7
T1102 A10	15.2	0.7	15.0	1.1	14.1	0.7
T664 A1	15.0	0.7	14.7	0.7	14.5	2.4

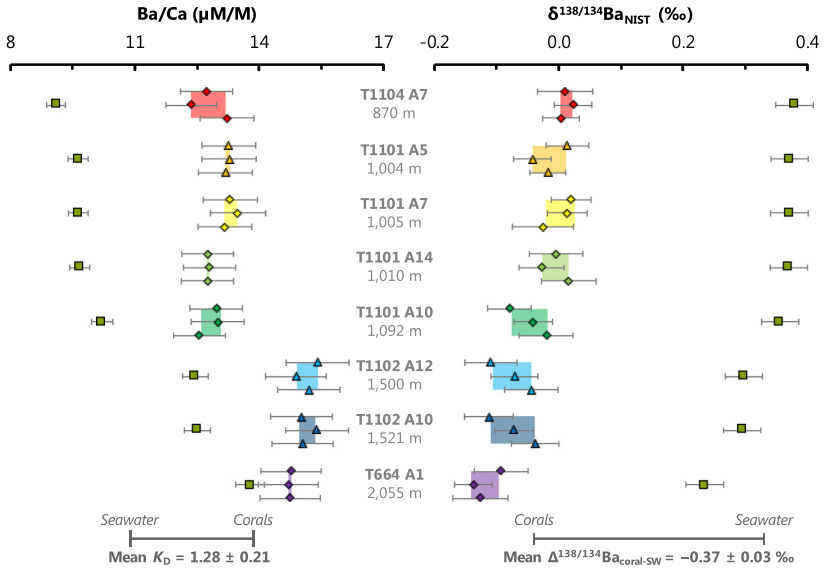

Fig. 4. Barium partitioning between seawater (squares) and deep-sea bamboo corals (diamonds [*Isidella*] and triangles [*Keratoisis*]). All modern coral edge samples exhibit Ba/Ca in excess of—and $\delta^{138/134}Ba_{NIST}$ lighter than—their respective ambient dissolved seawater, which was estimated via linear interpolation (see text for details). Shading illustrates (unweighted) mean and ±2 SE variability for each set of three edge replicates. The variability between edge replicates from a single coral specimen is similar to, or less than, our long-term ±2 SD measurement precision for both Ba/Ca (±4.9%) and $\delta^{138/134}Ba_{NIST}$ (±0.03‰), indicating that skeletal Ba chemistry is homogeneous within the outermost band (i.e., most recent growth).

Ba/Ca variability ranges from 0.2–2.8% RSD (mean of ±1.1%) for modern edges and 2–6% RSD (mean of ±3.5%) for historical interior samples, compared with ∼20% inter-specimen variability. Likewise, intra-specimen 2 SD variability in $\delta^{138/134}Ba_{NIST}$ ranges from ±0.02–0.06‰ (mean of ±0.04‰) for modern edges and ±0.02–0.04‰ (mean of ±0.03‰) for historical interior samples, compared with 0.15‰ inter-specimen variability.

Inter-specimen mean Ba/Ca and $\delta^{138/134}Ba_{NIST}$ exhibit systematic trends with respect to both ambient dissolved $[Ba]_{SW}$ and $\delta^{138/134}Ba_{NIST}$. We use two properties, $K_D{}^{Ba}$ and $\Delta^{138/134}Ba_{coral\text{-}SW}$, to describe these trends. Both properties are unitless, though we report $\Delta^{138/134}Ba_{coral\text{-}SW}$ in ‰ for consistency with Eq. 1. The first property, $K_D{}^{Ba}$:

$$K_D{}^{Ba} = (Ba/Ca)_{coral}/(Ba/Ca)_{SW} \quad (2)$$

illustrates whether corals possess Ba/Ca in excess ($K_D{}^{Ba} > 1$) or below ($K_D{}^{Ba} < 1$) that of their environment. Ambient seawater Ba/Ca was estimated by linear interpolation of California Margin $[Ba]_{SW}$ to the coral depths, and by normalizing to $[Ca]_{SW} = 10.3$ mM (Culkin and Cox, 1966). At 1,000 m, however, we assumed $[Ba]_{SW} = 98.1$ nmol/kg (from SAFe) in place of the oceanographically-inconsistent *in situ* value (Sec. 3.1). Likewise, for specimens collected below 1,500 m, ambient $[Ba]_{SW}$ was estimated by interpolation from SAFe. All corals possess Ba/Ca above ambient seawater (Fig. 6). The specimens exhibit a mean $K_D{}^{Ba} = 1.28\pm0.21$ (±2 SD; $n = 8$), though a depth dependence is evident: $K_D{}^{Ba}$ decreases from a maximum value of 1.40±0.09 at 870 m to 1.07±0.03 at 2,055 m, equivalent to a linear change of −0.27±0.07 per km (±2 SD, $R^2 = 0.92$; $n = 8$). The specimen mean—and depth dependent changes in—$K_D{}^{Ba}$ are robust regardless of whether the $[Ba]_{SW}$ at 1,000 m is from SAFe or the California Margin.

The second property, $\Delta^{138/134}Ba_{coral\text{-}SW}$:

$$\Delta^{138/134}Ba_{coral-SW} = (\delta^{138/134}Ba_{NIST})_{coral} - (\delta^{138/134}Ba_{NIST})_{SW} \quad (3)$$

indicates whether corals possess 'lighter' (i.e., enriched in ^{134}Ba; $\Delta^{138/134}Ba_{coral\text{-}SW} < 0$) or 'heavier' (i.e., enriched in ^{138}Ba; $\Delta^{138/134}Ba_{coral\text{-}SW} > 0$) Ba-isotopic compositions than ambient seawater. Ambient dissolved $\delta^{138/134}Ba_{NIST}$ was estimated in analogous manner to Ba/Ca, though we did not substitute the value at 1,000 m with that from SAFe, since evaporation should not impact $\delta^{138/134}Ba_{NIST}$. All specimens possess $\delta^{138/134}Ba_{NIST}$ lighter than ambient seawater (Fig. 6) with mean $\Delta^{138/134}Ba_{coral\text{-}SW} =$

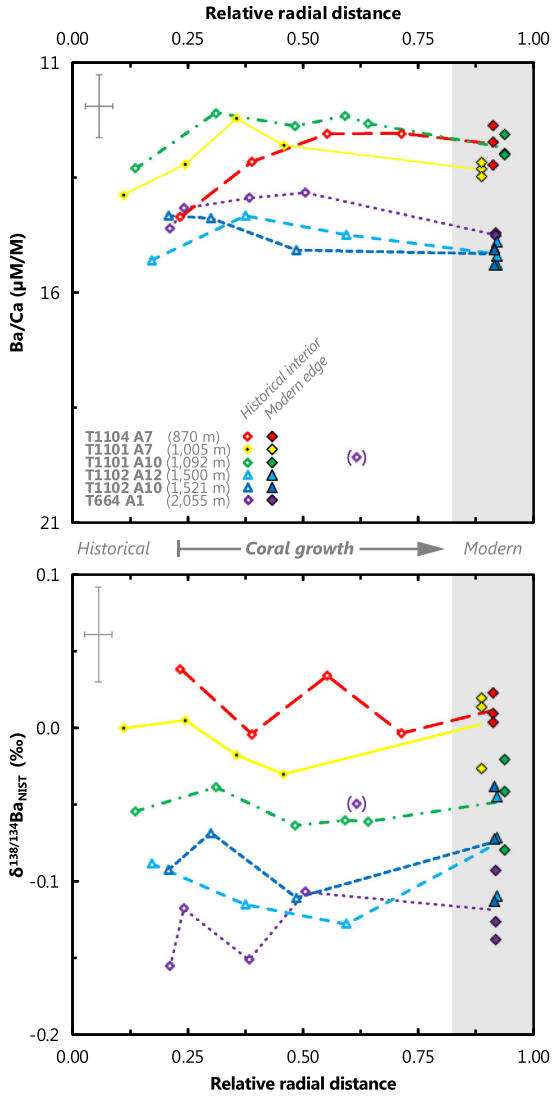

Fig. 5. Historical coral interior barium chemistry. Upper panel shows Ba/Ca (note reverse scale) and lower panel $\delta^{138/134}Ba_{NIST}$ against relative radial distance in coral, whereby unity represents the most recent growth. All specimens exhibit historical values that are within analytical uncertainty of their respective modern edge composition, except for a single datum from T664 A1, which is suspected of contamination (denoted by brackets; see text). Typical measurement uncertainty and sampling interval are shown in the upper-left of each panel.

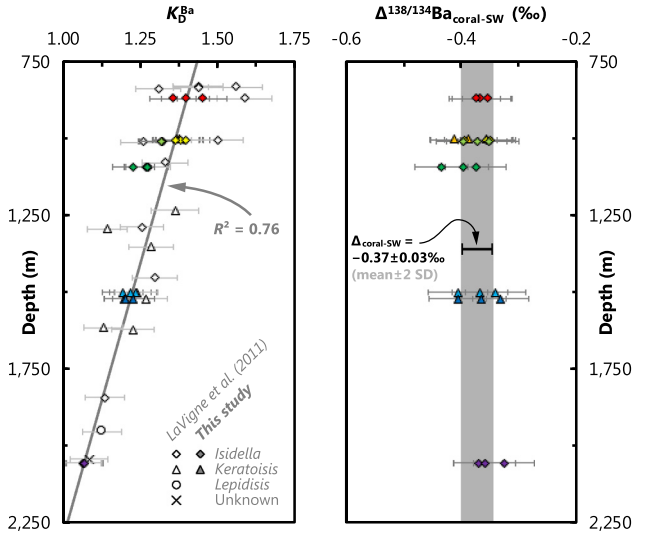

Fig. 6. Divergent depth-dependent patterns of barium partitioning. Using the mean coral edge samples from *this study* and the renormalized data from LaVigne et al. (2011), the partition coefficient for Ba, K_D^{Ba}, exhibits a change of −0.28±0.07 per km (solid line; slope uncertainty is ±2 SD, $n = 22$ unique specimens). Unlike K_D^{Ba}, $\Delta^{138/134}Ba_{coral\text{-}SW}$ exhibits no statistically-significant depth dependency, supporting the use of a fixed offset over the entire depth range of −0.37 ±0.03‰ ($n = 8$; vertical shading).

−0.37±0.03‰ (±2 SD; $n = 8$). Unlike K_D^{Ba}, $\Delta^{138/134}Ba_{coral\text{-}SW}$ exhibits no depth dependence.

4. Discussion

4.1. Phase associations

Bamboo corals exhibit Ba/Ca that scales with that of ambient seawater (e.g., LaVigne et al., 2011; Thresher et al., 2016; Flöter et al., 2019). While $K_D^{Ba} \geq 1$ is consistent with that of other deep sea and surface-dwelling aragonitic corals, this value is somewhat unusual for calcite (LaVigne et al., 2016). This enrichment could derive from calcification if there were a mineralogical preference for Ba over Ca in high-Mg calcite, or if bamboo coral physiological processes significantly modulate skeletal Ba/Ca. Alternatively, this enrichment could derive from incorporation of extraneous Ba, which could be important considering that deep-sea corals are filter feeders that rely on sinking particulate organic matter for energy (Griffin and Druffel, 1989; Sherwood and Risk, 2007). Moreover, these corals inhabit mesopelagic depths where discrete micron-sized $BaSO_4$ crystals are abundant (Dehairs et al., 1980). To discriminate between these interpretations, we tested whether any of the Ba associated with deep-sea coral high-Mg calcite originates from ambient particulate matter, which could be endogenously (e.g., organic matter) or exogenously produced (e.g., $BaSO_4$).

The stepped cleaning test did not result in any changes in Ba/Ca that exceeded analytical precision (Table 2). Likewise, SEM analyses revealed no evidence for encased $BaSO_4$ crystals associated with the corals, in accord with the findings of Flöter et al. (2019). Our results are consistent with the high-Mg calcite skeleton being the dominant Ba host phase in deep-sea bamboo corals and suggest that neither oxidative nor alkaline DTPA chemical cleaning are necessary for obtaining reliable Ba/Ca and—by extension—Ba-isotopic data. Accordingly, we did not perform chemical cleaning on historical interior samples that were subsampled after the conclusion of the cleaning experiment. Despite performing the cleaning on the modern edge samples subject to Ba-isotopic analysis, two lines of evidence lead us to believe that these data are comparable with the historical interior samples: there are no systematic offsets in Ba/Ca between treated and untreated powders (Sec. 3.2.1), meaning that it is unlikely that cleaning rendered any significant effect on measured Ba-isotopic chemistry; and, the untreated historical interior samples exhibit essentially identical Ba-isotopic compositions to their respective modern edges (Sec. 3.2.2). Thus, we conclude that neither inter-crystalline organic matter nor encased $BaSO_4$ significantly contribute to the Ba content of live-collected deep-sea bamboo corals. Fossil specimens, particularly those with well-developed Fe-Mn coating, may require additional reductive cleaning.

By ruling out extraneous Ba, we are left with calcification as the driver behind elevated K_D^{Ba}, though the mechanism is uncertain. While it is possible that ionic substitution of Ba becomes more favorable as calcite Mg/Ca increases (akin to Sr; e.g., Mucci and Morse, 1983), physiological modulation of K_D^{Ba} is also plausible considering culture data; benthic high-Mg calcite foraminifera exhibit K_D^{Ba} both below and above unity, depending on species (cf. Hintz et al., 2006; Dijk et al., 2017). These results leave open

the possibility that equilibrium K_D^{Ba} for high-Mg calcite is below unity, which could be tested by examining Ba partitioning during inorganic calcite precipitation across a range of solid Mg/Ca.

4.2. Barium partitioning

4.2.1. Barium distributions in the northeast Pacific

To facilitate evaluation of K_D^{Ba} and $\Delta^{138/134}Ba_{coral\text{-}SW}$ in the corals, we measured two profiles of dissolved $[Ba]_{SW}$ and $\delta^{138/134}Ba_{NIST}$ from the northeast Pacific. Taken together, both profiles show depth-dependent patterns consistent with those emerging from other marine Ba-isotopic datasets. Much of the open ocean falls on a single, linear array in $\delta^{138/134}Ba_{NIST}$–$1/[Ba]_{SW}$ space (Fig. 3; Horner et al., 2015), albeit with a few notable exceptions discussed in detail elsewhere (e.g., Bates et al., 2017; Hsieh and Henderson, 2017). In general, Ba-replete ($\geq$100 nM) waters are characterized by light $\delta^{138/134}Ba_{NIST} \approx +0.3‰$, and Ba-depleted surface waters (<40 nM) possess $\delta^{138/134}Ba_{NIST} \approx +0.6‰$. Most samples from the northeast Pacific fall between these two end-members. However, the most Ba-rich samples from SAFe ($\approx$150 nM)—between 2,000–4,000 m, corresponding to the core of PDW—extend this array to $\delta^{138/134}Ba_{NIST} \approx +0.2‰$, which is lighter than previously reported open-marine compositions (Fig. 3).

We suspect that the high $[Ba]_{SW}$ and light $\delta^{138/134}Ba_{NIST}$ of PDW originates through the interplay between $BaSO_4$ cycling and the unique regional hydrography. Northeast Pacific overturning circulation is weak (Talley, 2008). Weaker deep circulation promotes greater accumulation of regenerated particulate matter compared to deep waters with stronger overturning circulation, such as the Atlantic. Silicon, which exhibits a similar marine distribution to Ba, exhibits a maximum in its regenerated inventory in northeast Pacific deep waters (e.g., de Souza et al., 2014). By analogy, we posit that PDW has similarly accumulated significant quantities of regenerated $BaSO_4$, rendering higher $[Ba]_{SW}$ and lighter $\delta^{138/134}Ba_{NIST}$ than deep waters from the Southern or Atlantic Oceans (e.g., Bates et al., 2017; Hsieh & Henderson, 2017). That PDW exhibits Ba^* $\sim$0 nmol/kg suggests that Ba and Si were accumulated, on average, in proportion to the slope of global [Ba]–[Si] relationship ($\approx$0.63 mmol/mol; Bates et al., 2017; Fig. 2), which is unsurprising considering that this relationship is itself strongly influenced by the [Ba]:[Si] ratio of PDW. Above and below PDW, however, dissolved Ba–Si decoupling is more pronounced. At depths corresponding to NPIW/AAIW/UCDW in the mesopelagic, there is a distinct minimum in Ba^* coincident with that of $[O_2]$ at both SAFe and along the California Margin (Fig. 2). Low $[O_2]$ indicates a combination of poor ventilation and organic matter respiration, whereby the latter lowers $[Ba]_{SW}$—but not [Si]—through $BaSO_4$ formation. Likewise, in the abyssal ocean at SAFe, Ba^* exhibits a maximum associated with LCDW, presumably reflecting mixing with southern-sourced water masses that are enriched in Ba relative to Si.

Lastly, in addition to highlighting the importance of hydrography to bathypelagic marine Ba-isotopic chemistry, our new seawater profiles reinforce the importance of circulation in the mesopelagic, even in regions that are poorly ventilated. Above 1,000 m, gradients in Ba-related properties are steeper along the California Margin compared to SAFe; this shoaling of the 'baricline' is concomitant with a general shoaling of NPIW (Fig. 1). Below $\approx$1,000 m isopycnal surfaces are essentially flat (Talley, 2008); for a given depth, all Ba-related properties exhibit similar values across the northeast Pacific (Fig. 2). Thus, we conclude that intermediate and deep northeast Pacific Ba chemistry is similarly strongly coupled to regional circulation, as with the Atlantic and Southern Oceans (e.g., Horner et al., 2015; Bates et al., 2017; Hsieh and Henderson, 2017; Hemsing et al., 2018).

4.2.2. Depth-dependence of K_D^{Ba}

All corals possess $K_D^{Ba} > 1$, in agreement with data from other types of deep-sea coral recovered from the Pacific and elsewhere (e.g., LaVigne et al., 2011; Thresher et al., 2016; Spooner et al., 2018). In detail however, K_D^{Ba} varies systematically with depth, ranging from $\approx$1.4 at 870 m to $\approx$1.1 at 2,055 m (Fig. 6). Nearby corals analyzed by LaVigne et al. (2011) show a similar depth dependence when renormalized to our more proximal seawater profile, with K_D^{Ba} decreasing from $\approx$1.6 to $\approx$1.1 over an equivalent depth range. There do not appear to be any systematic taxonomic-related effects on K_D^{Ba} nor any correlation between K_D^{Ba} and Mg/Ca or Sr/Ca (Fig. S5). Since six of the eight specimens analyzed here were previously measured by LaVigne et al. (2011), we can directly compare Ba/Ca measured by two laboratories (WHOI and UC Davis), using different instrumentation (quadrupole versus sector-field ICP-MS), and sample sizes (15 versus 1 mg). The average difference in Ba/Ca is less than 5 %—similar to our long-term measurement precision—indicating that the data are directly comparable. An unweighted linear regression of specimen average K_D^{Ba} versus depth yields a gradient of -0.28 ± 0.07 per km (±2 SD, $n = 24$; $R^2 = 0.76$), implying that deeper-dwelling corals incorporate significantly less Ba, relative to Ca, compared to shallower-dwelling specimens.

Depth-dependent variations in K_D have been reported for other trace cations in biogenic calcites, particularly for Ba, Cd, and Sr partitioning into benthic forams (e.g., Boyle, 1992; McCorkle et al., 1995). Such variations are thought to arise through one—or a combination—of two mechanisms: selective dissolution during prolonged exposure to calcite-undersaturated seawater or from depth-dependent differences in Ba partitioning during calcification. Though the specimens studied here all dwell in calcite-undersaturated waters (e.g., Feely et al., 2002), selective dissolution seems unlikely. Most corals were collected with living polyps, indicating short exposure times (i.e., less than a century; Table 1) and $\Omega_{calcite}$ is essentially invariant over the depths spanned by the specimens (Fig. S6). Alternatively, the systematic partitioning trend may reflect depth-dependent changes in the equilibrium thermodynamic- or physiologically-mediated partitioning of Ba into deep-sea bamboo coral calcite. Equilibrium thermodynamic controls on K_D are a well-established concept, whereby K_D tends toward unity at higher temperatures (e.g., Gaetani and Cohen, 2006; Gonneea et al., 2017) and decreases with pressure (e.g., Boyle, 1992; McCorkle et al., 1995). Regarding temperature, the pattern exhibited by deep-sea bamboo corals is the opposite of that expected: both K_D^{Ba} (Fig. 6) and T (Fig. S4) decrease with depth, indicating that temperature is not the dominant factor modulating the depth dependence. While the observed depth-dependence of K_D^{Ba} is consistent with a pressure effect, other calcitic tests show no effect (e.g., low-Mg calcite foraminifera; Lea and Boyle, 1989; Boyle, 1992) and we are not aware of any laboratory tests into this phenomenon for Ba. Thus, a physiological explanation is also possible, and perhaps even likely given that all specimens precipitate from seawater that is undersaturated with respect to calcite (Feely et al., 2002). Physiological effects would imply that the corals exhibit systematically different calcification 'efficiencies' at different depths (e.g., Elderfield et al., 1996; Gagnon et al., 2012). If this model is appropriate for bamboo corals, lower K_D^{Ba} implies more efficient calcification with depth; the amount of calcite precipitated, relative to the turnover (or 'flushing') of the calcification fluid, is greater for deeper dwelling specimens. Since all specimens exhibit relatively similar average annual precipitation rates of $\approx4\pm2$ mm^2/yr (excepting the fast-growing specimen from 870 m; $\approx14\pm2$ mm^2/yr; Frenkel et al., 2017), increases in calcification efficiency must be driven by lower rates of turnover of the calcification fluid at greater depths. Why this turnover decreases with depth is more difficult to answer. Sea-

water properties relevant to coral physiology, such [O_2], nutrients, T, food supply, and alkalinity are all correlated with depth over the profile spanned by the corals (see Fig. S4). Thus, we cannot yet isolate a unique driving mechanism for the observed depth-dependent partitioning of Ba into northeast Pacific bamboo corals, though we encourage additional efforts to do so.

Regardless of the mechanism, the Ba/Ca of recently-collected corals can be related to ambient Ba chemistry if accounting for the depth dependence of K_D^{Ba}. We define the following empirical expression that relates the Ba/Ca of northeast Pacific deep-sea bamboo corals to $[Ba]_{SW}$, over the domain spanned by the corals (870–2,055 m):

$$[Ba]_{SW} = 10.3 \times (Ba/Ca)_{coral}/[1.64 - 0.28 \times z] \quad (4)$$

where $[Ba]_{SW}$, $(Ba/Ca)_{coral}$, and z are in units of nM, μmol/mol, and km, respectively. In the absence of a larger sample set, it is difficult to independently test the precision and accuracy of Eq. 4 to estimate $[Ba]_{SW}$. We can obtain a relatively crude estimate of precision by comparing reconstructed $[Ba]_{SW}$ from corals recovered at similar depths, since such specimens should all be bathed by the same water. Performing this comparison with specimens T1101 A5, T1101 A7, and T1101 A14 (from 1,004, 1,005, and 1,010 m, respectively; Table 1) yields a range of $[Ba]_{SW}$ estimates spanning 97–101 nM, implying a minimum estimation precision on the order of ±3% (±RSD). We note, however, that using Eq. 4 to estimate $[Ba]_{SW}$ for fossil corals recovered *in situ* implicitly assumes that the factors driving the depth dependence have also remained constant through time. Since these factors are presently unknown, the accuracy of Eq. 4 in the past is uncertain.

4.2.3. Invariance of $\Delta^{138/134}Ba_{coral-SW}$

All deep-sea bamboo corals exhibit Ba-isotopic compositions lighter than ambient seawater. The (unweighted) specimen average $\Delta^{138/134}Ba_{coral\text{-}SW} = -0.37 \pm 0.03$‰ (mean±2 SD; $n = 8$). Unlike K_D^{Ba}, however, $\Delta^{138/134}Ba_{coral\text{-}SW}$ exhibits no depth dependence and is thus presumably also insensitive to environmental variables (Fig. 5, 6). Interpreted alongside the coral growth rate measurements, invariance of coral interior $\delta^{138/134}Ba_{NIST}$ similarly precludes any dependence between $\Delta^{138/134}Ba_{coral\text{-}SW}$ and growth rate within individual specimens. Likewise, there are no obvious differences in $\Delta^{138/134}Ba_{coral\text{-}SW}$ between taxa inhabiting similar depths; variability between specimens T1101 A5 (*Keratoisis*), T1101 A7 (*Isidella*), and T1101 A14 (*Isidella*; from 1,004, 1,005, and 1,010 m, respectively) is only ±0.01‰ (±2 SD, $n = 3$), which is significantly less than our long-term precision of ±0.03‰. That K_D^{Ba} systematically varies along the profile, and $\Delta^{138/134}Ba_{coral\text{-}SW}$ does not, may indicate that any changes in calcification efficiency between specimens is insufficient to render resolvable changes in $\Delta^{138/134}Ba_{coral\text{-}SW}$. Thus, we conclude that ambient Ba-isotopic chemistry is the dominant control on deep-sea bamboo coral $\delta^{138/134}Ba_{NIST}$, rather than any factor intrinsic to the coral.

Then what drives $\Delta^{138/134}Ba_{coral\text{-}SW}$ for deep-sea bamboo corals? A likely possibility is that $\Delta^{138/134}Ba_{coral\text{-}SW}$ is set by a mineralogical effect during Ba partitioning into high-Mg calcite. Recent studies showed that different Ba-bearing minerals exhibit different $\Delta^{138/134}Ba$ (i.e., mineral–fluid isotopic separation factors), ranging from −0.09±0.05‰ for witherite ($BaCO_3$; Mavromatis et al., 2016), −0.32±0.03‰ for $BaSO_4$ precipitated at low pH (von Allmen et al., 2010), and ≈ −0.5‰ implied for marine $BaSO_4$ (e.g., Horner et al., 2017; Bridgestock et al., 2018; Crockford et al., 2019). Of most relevance to this study is a recent core-top calibration using deep-sea aragonitic corals, which yielded a mean $\Delta^{138/134}Ba_{coral\text{-}SW}$ of −0.21±0.08‰ (Hemsing et al., 2018). Though the aragonitic deep-sea coral offset is markedly smaller than observed here for high-Mg calcitic deep-sea (bamboo) corals, the offset is similarly insensitive to ambient environmental variables (Hemsing et al., 2018). While existing Ba-isotopic data for deep-sea corals are consistent with a mineralogical control on $\Delta^{138/134}Ba_{coral\text{-}SW}$, definitive confirmation will require inorganic $CaCO_3$ precipitation experiments, and in particular those where Ba is a trace constituent of the resultant precipitate.

The depth- and taxonomic-invariance of $\Delta^{138/134}Ba_{coral\text{-}SW}$ suggests that deep-sea bamboo corals are potentially valuable archives of past marine Ba-isotopic chemistry. We thus put forth the following empirical relation that enables converting coral $\delta^{138/134}Ba_{NIST}$ to historical seawater Ba-isotopic compositions:

$$(\delta^{138/134}Ba_{NIST})_{SW} = (\delta^{138/134}Ba_{NIST})_{coral} + 0.37‰ \quad (5)$$

where all properties are unitless. Assuming a typical measurement uncertainty of ±0.03‰, Eq. 5 yields estimates of $(\delta^{138/134}Ba_{NIST})_{SW}$ to within ±0.04‰. Thus, paired measurements of Ba/Ca and $\delta^{138/134}Ba_{NIST}$ in deep-sea bamboo corals can inform on past changes in $[Ba]_{SW}$ and dissolved $\delta^{138/134}Ba_{NIST}$, respectively. Unlike Ba/Ca however, use of $\delta^{138/134}Ba_{NIST}$ is free from uncertainties regarding the factors driving depth-dependent variations in K_D^{Ba}. Such variations may diminish the accuracy of $[Ba]_{SW}$ estimates, but not those of $\delta^{138/134}Ba_{NIST}$.

4.3. Paleoceanographic prospects

Here we explore how paired measurement of Ba/Ca and $\delta^{138/134}Ba_{NIST}$ might be used to interrogate past ocean chemistry by examining the skeletal chemistry of historical growth bands in six of the eight corals used in the modern calibration (Table 1). A single subsample from T664 A1 is excluded from this discussion as we suspect the powder may have been contaminated during micromilling (Fig. 5, relative radial distance of ≈0.62). The Ba/Ca (and $\delta^{138/134}Ba_{NIST}$) of this subsample is significantly elevated above the specimen mean, whereas no such Ba/Ca feature was observed during high-resolution LA-ICP-MS mapping (Serrato Marks et al., 2017). Excluding this subsample, historical intra-specimen variations in skeletal Ba chemistry are significantly smaller than the inter-specimen range. Even so, a subtle depth-dependent pattern is evident, whereby intra-specimen variability in Ba/Ca decreases monotonically from ±5.6 to ±2.1% RSD over the profile. (Mean historical intra-specimen variability in $\delta^{138/134}Ba_{NIST}$ is equivalent to current measurement precision of ±0.03‰, and so we cannot confidently identify any systematic trends.) Interior skeletal Ba/Ca variability outside of our measurement precision of ±2.5% RSD requires temporal variations in either ambient $[Ba]_{SW}$ or K_D^{Ba}. We consider the former as relatively unlikely, given that a profile of northeast Pacific $[Ba]_{SW}$ from the nearest GEOSECS station, collected in 1973, is essentially identical to that obtained at SAFe in 2009 (Fig. 1). Thus, temporal changes in K_D^{Ba} are required to explain the interior Ba/Ca variability, discussed in detail elsewhere (e.g., Serrato Marks et al., 2017; Flöter et al., 2019). That the relative amount of intra-specimen Ba/Ca variability shows a depth dependence could indicate that it is related to the same processes governing the inter-specimen gradient in K_D^{Ba}. Regardless of any gradients in intra-specimen variability, the mean Ba/Ca and $\delta^{138/134}Ba_{NIST}$ of the historical interior subsamples are identical, within uncertainty, to their respective modern edges (Fig. 5). Since we do not expect significant variability in northeast Pacific $[Ba]_{SW}$ and $\delta^{138/134}Ba_{NIST}$ over the last century, we interpret the general absence of interior skeletal variability as evidence of the reliability of deep-sea bamboo corals to record ambient Ba chemistry over their long lifespans.

Overall, our data suggest a relatively simple framework for interpreting Ba/Ca and Ba-isotopic records recovered from deep-sea bamboo corals: the former reflects ambient Ba/Ca with a

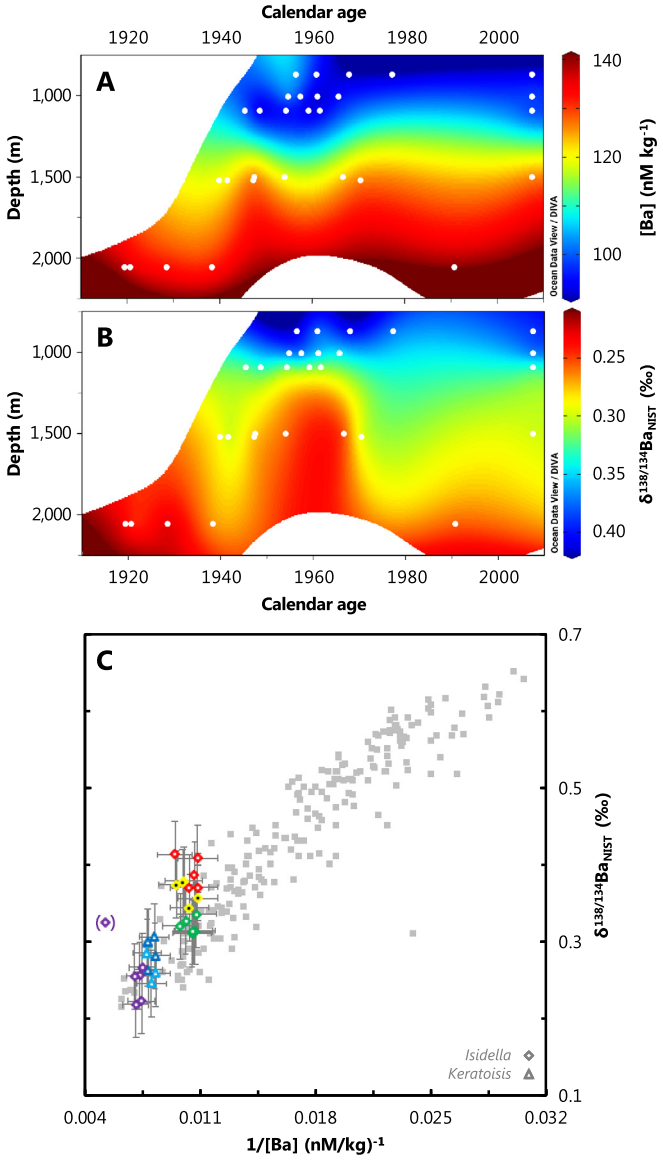

Fig. 7. One-hundred year record of northeast Pacific barium chemistry. Time-resolved profiles of reconstructed [Ba] (A) and $\delta^{138/134}Ba_{NIST}$ (B), based on historical interior data (Fig. 5) and our calibration (Fig. 6). Calendar ages were assigned from published and new radiocarbon measurements (Frenkel et al., 2017; Supplement). Bottom panel (C) shows data from (A) and (B) in property–property space overlaying modern seawater data (squares; data sources as in Fig. 3). Symbology as in Fig. 5. The subsample suspected of contamination from T664 A1 has been omitted from panels A and B, and is indicated by parentheses in panel C. Aside from this subsample, deep-sea bamboo corals appear to be reliable recorders of ambient Ba chemistry over their lifespans and reflect the general trend seen in modern meso- and bathypelagic seawater samples.

depth-dependent partition coefficient (Eq. 4), and the latter reflects ambient $\delta^{138/134}Ba_{NIST}$ with a depth-invariant offset (Eq. 5). Accordingly, we can combine our measurements of skeletal Ba chemistry across multiple specimens with paired radiocarbon ages to construct time- and depth-resolved patterns of past seawater chemistry (Fig. 7). Such records may find utility in studying patterns of ocean circulation over multi-decadal to millennial timescales, and we outline four such potential applications here. First, paired measurement of Ba/Ca and $\delta^{138/134}Ba_{NIST}$ enables reconstruction of the relationship between $\delta^{138/134}Ba_{NIST}$–1/[Ba] through time (Fig. 7). As noted by Hemsing et al. (2018), this slope should be sensitive to whole-ocean changes in marine Ba cycling. Second, the modern distribution of $\delta^{138/134}Ba_{NIST}$ strongly depends on ocean mixing, even in the northeast Pacific, where the overturning circulation is weak. Thus, depth-resolved records of $\delta^{138/134}Ba_{NIST}$ harbor potential to reveal the geometry of past ocean circulation. Third, should the depth-dependent variability in Ba/Ca and $\delta^{138/134}Ba_{NIST}$ be found to relate to ambient seawater and not skeletal architecture, high-resolution sampling of deep-sea corals may enable reconstruction of transient ocean circulation changes, such as those associated with episodes of rapid climate change (e.g., Adkins et al., 1998). Finally, our data suggest that while K_D^{Ba} varies with depth, $\Delta^{138/134}Ba_{coral\text{-}SW}$ is constant over the same gradient in environmental conditions. Estimation of past ocean $\delta^{138/134}Ba_{NIST}$ is therefore free of the main assumption inherent in estimating past $[Ba]_{SW}$: that the modern depth-dependency of K_D^{Ba} holds true in the past. Such an assumption could also be inverted, however, should the $\delta^{138/134}Ba_{NIST}$–$1/[Ba]_{SW}$ relationship have remained similar through time: $\delta^{138/134}Ba_{NIST}$ could be used to independently estimate past $[Ba]_{SW}$ (i.e., from Figs. 3 & 7). The difference between Ba/Ca- and $\delta^{138/134}Ba_{NIST}$-derived estimates of $[Ba]_{SW}$ may serve as a proxy for the control variable modulating K_D^{Ba}. This postulate reinforces our earlier call for additional efforts to identify the variable controlling depth-dependent variations in Ba partitioning.

5. Summary

We present a comprehensive assessment of extant and emerging Ba-based proxies in calcitic deep-sea corals from the northeast Pacific. To facilitate this assessment, we report the first full-ocean depth profiles of Ba-isotopic chemistry from the Pacific Ocean at SAFe and a composite profile close to the California Margin. We find systematic depth-dependent variations in $\delta^{138/134}Ba_{NIST}$ at both sites that strongly correlate with regional hydrography, including identification of a global Ba-isotopic minimum at the Ba-rich core of PDW. The results support an emerging paradigm that modern marine Ba-isotopic distributions are largely driven by patterns of basin-scale circulation. Using a stepped cleaning experiment and high-resolution imaging, we rule out the contribution of extraneous Ba phases to the Ba inventory of bamboo corals. The average Ba/Ca of eight northeast Pacific bamboo corals reflects ambient $[Ba]_{SW}$. A compilation of new and existing Ba/Ca data indicates that the partition coefficient, K_D^{Ba}, systematically changes by -0.28 ± 0.07 per km. The underlying mechanism is unresolved. Unlike K_D^{Ba}, Ba-isotopic partitioning exhibits no depth dependence, with $\Delta^{138/134}Ba_{coral\text{-}SW}$ constant for all eight specimens at -0.37 ± 0.03‰. Similarly, $\Delta^{138/134}Ba_{coral\text{-}SW}$ remained stable over the lifespans of six radiometrically-dated corals. As such, time-resolved records of skeletal Ba-isotopic chemistry may be solely interpreted in terms of past seawater $\delta^{138/134}Ba_{NIST}$. We conclude that deep-sea bamboo corals are useful archives for reconstructing past variations in marine Ba chemistry and, by extension, the geometry of past ocean circulation.

Data access

Seawater data are available through the Biological and Chemical Oceanography Data Management Office (doi:10.1575/1912/bco-dmo.770368.2 and doi:10.1575/1912/bco-dmo.770447.1 for KN195-08 and MV1405, respectively). Coral data are tabulated in the Supplement and are available from NOAA's National Centers for Environmental Information (www.ncdc.noaa.gov/paleo-search/study/27170).

Author contributions

M.L. and T.J.H. conceived and designed the study; B.M.G., J.L.P., and T.J.H. acquired data; all authors analyzed data; and, all authors drafted the manuscript.

Acknowledgements

Tremendous thanks to Claire Till (HSU) and Tessa Hill (UCD) for sharing samples; Mark Brzezinski (UCSB) for early access to dissolved [Si] data; Maureen Auro (WHOI) for keeping the labs running; Sune Nielsen (WHOI) for discussions; Gretchen Swarr and Jerzy Blusztajn for assistance in the WHOI Plasma Facility; Emily Peterman for facilitating SEM access at Bowdoin College; Chief Scientists David Clague (MBARI), Greg Cutter (ODU), and Ken Bruland (UCSC) for masterminding sample collection during Seamounts 2004 and 2007, KN195-08, and MV1405, respectively; and, an anonymous referee and Susan Little for constructive comments that improved the manuscript. We gratefully acknowledge grants from the National Science Foundation, which provided a WHOI Summer Student Fellowship for B.M.G. (OCE-1156952), undergraduate research fellowships to B.M.G. and J.L.P. (OCE-1420984, to M.L.), and support isotope research in the NIRVANA Labs (OCE-1443577 and OCE-1736949, to T.J.H.).

Appendix A. Supplementary material

Supplementary material related to this article can be found online at https://doi.org/10.1016/j.epsl.2019.115751.

References

Adkins, J.F., 2013. The role of deep ocean circulation in setting glacial climates. Paleoceanography 28 (3), 539–561. https://doi.org/10.1002/palo.20046.

Adkins, J.F., Cheng, H., Boyle, E.A., Druffel, E.R.M., Edwards, R.L., 1998. Deep-sea coral evidence for rapid change in ventilation of the deep North Atlantic 15,400 years ago. Science 280 (5364), 725. https://doi.org/10.1126/science.280.5364.725, LP-728.

Bates, S.L., Hendry, K.R., Pryer, H.V., Kinsley, C.W., Pyle, K.M., Woodward, E.M.S., Horner, T.J., 2017. Barium isotopes reveal role of ocean circulation on barium cycling in the Atlantic. Geochim. Cosmochim. Acta 204, 286–299. https://doi.org/10.1016/j.gca.2017.01.043.

Bishop, J.K.B., 1988. The barite-opal-organic carbon association in oceanic particulate matter. Nature 332, 341–343. https://doi.org/10.1038/332341a0.

Boyer, T.P., Baranova, O.K., Coleman, C., García, H.E., Grodsky, A., Locarnini, R.A., Mishonov, A.V., Paver, C.R., Reagan, J.R., Seidov, D., Smolyar, I.V., Weathers, K.W., Zweng, M.M., 2018. World Ocean Database 2018. Mishonov, A.V. (Technical Editor), NOAA Atlas NESDIS 87.

Boyle, E.A., 1992. Cadmium and δ^{13}C paleochemical ocean distributions during the stage 2 glacial maximum. Annu. Rev. Earth Planet. Sci. 20 (1), 245–287. https://doi.org/10.1146/annurev.ea.20.050192.001333.

Bridgestock, L., Hsieh, Y.T., Porcelli, D., Homoky, W.B., Bryan, A., Henderson, G.M., 2018. Controls on the barium isotope compositions of marine sediments. Earth Planet. Sci. Lett. 481, 101–110. https://doi.org/10.1016/j.epsl.2017.10.019.

Chan, L.H., Edmond, J.M., Stallard, R.F., Broecker, W.S., Chung, Y.C., Weiss, R.F., Ku, T.L., 1976. Radium and barium at GEOSECS stations in the Atlantic and Pacific. Earth Planet. Sci. Lett. 32 (2), 258–267. https://doi.org/10.1016/0012-821X(76)90066-2.

Chow, T.J., Goldberg, E.D., 1960. On the marine geochemistry of barium. Geochim. Cosmochim. Acta 20 (3–4), 192–198. https://doi.org/10.1016/0016-7037(60)90073-9.

Crockford, P.W., Wing, B.A., Paytan, A., Hodgskiss, M.S., Bitterwolf, K.K., Hayles, J.A., Middleton, J.E., Ahm, A.-S., Johnston, D.T., Caxito, F., Uhlein, G., Halverson, G.P., Eickmann, B., Torres, M., Horner, T.J., 2019. Barium-isotopic constraints on the origin of post-Marinoan barites. Earth Planet. Sci. Lett. 519, 234–244. https://doi.org/10.1016/j.epsl.2019.05.018.

Culkin, F., Cox, R.A., 1966. Sodium, potassium, magnesium, calcium and strontium in seawater. Deep-Sea Res. Oceanogr. Abstr. 13 (5), 789–804. https://doi.org/10.1016/0011-7471(76)90905-0.

Cutter, G.A., Andersson, P., Codispoti, L., Croot, P., François, R., Lohan, M.C., Obata, H., Rutgers v. d. Loeff, M., 2010. Sampling and sample-handling protocols for GEOTRACES cruises. Eprint ID:34484. http://hdl.handle.net/10013/epic.42722.

de Souza, G.F., Slater, R.D., Dunne, J.P., Sarmiento, J.L., 2014. Deconvolving the controls on the deep ocean's silicon stable isotope distribution. Earth Planet. Sci. Lett. 398, 66–76.

Dehairs, F., Chesselet, R., Jedwab, J., 1980. Discrete suspended particles of barite and the barium cycle in the open ocean. Earth Planet. Sci. Lett. 49 (2), 528–550. https://doi.org/10.1016/0012-821X(80)90094-1.

Dijk, I.V., Nooijer, L.J.D., Reichart, G.J., 2017. Trends in element incorporation in hyaline and porcelaneous foraminifera as a function of pCO_2. Biogeosciences 14 (3), 497–510. https://doi.org/10.5194/bg-14-497-2017.

Elderfield, H., Bertram, C.J., Erez, J., 1996. A biomineralization model for the incorporation of trace elements into foraminiferal calcium carbonate. Earth Planet. Sci. Lett. 142 (3), 409–423. https://doi.org/10.1016/0012-821X(96)00105-7.

Farmer, J.R., Robinson, L.F., Hönisch, B., 2015. Growth rate determinations from radiocarbon in bamboo corals (genus Keratoisis). Deep-Sea Res., Part 1, Oceanogr. Res. Pap. 105, 26–40. https://doi.org/10.1016/j.dsr.2015.08.004.

Feely, R.A., Sabine, C.L., Lee, K., Millero, F.J., Lamb, M.F., Greeley, D., Bullister, J.L., Key, R.M., Peng, T.-H., Kozyr, A., Ono, T., Wong, C.S., 2002. In situ calcium carbonate dissolution in the Pacific Ocean. Glob. Biogeochem. Cycles 16 (4), 12–91. https://doi.org/10.1029/2002GB001866.

Flöter, S., Fietzke, J., Gutjahr, M., Farmer, J., Hönisch, B., Nehrke, G., Eisenhauer, A., 2019. The influence of skeletal micro-structures on potential proxy records in a bamboo coral. Geochim. Cosmochim. Acta 248, 43–60. https://doi.org/10.1016/j.gca.2018.12.027.

France, S.C., 2007. Genetic analysis of bamboo corals (Cnidaria: Octocorallia: Isididae): does lack of colony branching distinguish Lepidisis from Keratoisis? Bull. Mar. Sci. 81, 323–333.

Frenkel, M., LaVigne, M., Miller, H., Hill, T., McNichol, A., Lardie, M., 2017. Quantifying bamboo coral growth rate nonlinearity with the radiocarbon bomb spike: a new model for paleoceanographic chronology development. Deep-Sea Res. (I) 125, 26–39. https://doi.org/10.1016/j.dsr.2017.04.006.

Gaetani, G.A., Cohen, A.L., 2006. Element partitioning during precipitation of aragonite from seawater: a framework for understanding paleoproxies. Geochim. Cosmochim. Acta 70 (18), 4617–4634. https://doi.org/10.1016/j.gca.2006.07.008.

Gagnon, A.C., Adkins, J.F., Erez, J., 2012. Seawater transport during coral biomineralization. Earth Planet. Sci. Lett. 329, 150–161. https://doi.org/10.1016/j.epsl.2012.03.005.

Gonneea, M.E., Cohen, A.L., DeCarlo, T.M., Charette, M.A., 2017. Relationship between water and aragonite barium concentrations in aquaria reared juvenile corals. Geochim. Cosmochim. Acta 209, 123–134. https://doi.org/10.1016/j.gca.2017.04.006.

Griffin, S., Druffel, E., 1989. Sources of carbon to deep-sea corals. Radiocarbon 31 (3), 533–543. https://doi.org/10.1017/S0033822200012121.

Hathorne, E.C., et al., 2013. Interlaboratory study for coral Sr/Ca and other element/Ca ratio measurements. Geochem. Geophys. Geosyst. 14, 3730–3750. https://doi.org/10.1002/ggge.20230.

Hemsing, F., Hsieh, Y.T., Bridgestock, L., Spooner, P.T., Robinson, L.F., Frank, N., Henderson, G.M., 2018. Barium isotopes in cold-water corals. Earth Planet. Sci. Lett. 491, 183–192. https://doi.org/10.1016/j.epsl.2018.03.040.

Hill, T.M., Myrvold, C.R., Spero, H., Guilderson, T., 2014. Evidence for benthic-pelagic food web coupling and carbon export from California margin bamboo coral archives. Biogeosciences 11, 3845–3854. https://doi.org/10.5194/bgd-11-2595-2014.

Hintz, C.J., Shaw, T.J., Chandler, G.T., Bernhard, J.M., McCorkle, D.C., Blanks, J.K., 2006. Trace/minor element: calcium ratios in cultured benthic foraminifera. Part I: inter-species and inter-individual variability. Geochim. Cosmochim. Acta 70 (8), 1952–1963. https://doi.org/10.1016/j.gca.2005.12.018.

Horner, T.J., Kinsley, C.W., Nielsen, S.G., 2015. Barium-isotopic fractionation in seawater mediated by barite cycling and oceanic circulation. Earth Planet. Sci. Lett. 430, 511–522. https://doi.org/10.1016/j.epsl.2015.07.027.

Horner, T.J., Pryer, H.V., Nielsen, S.G., Crockford, P.W., Gauglitz, J.M., Wing, B.A., Ricketts, R.D., 2017. Pelagic barite precipitation at micromolar ambient sulfate. Nat. Commun. 8 (1), 1342. https://doi.org/10.1038/s41467-017-01229-5.

Hsieh, Y-T., Henderson, G.M., 2017. Barium stable isotopes in the global ocean: tracer of Ba inputs and utilization. Earth Planet. Sci. Lett. 473, 269–278. https://doi.org/10.1016/j.epsl.2017.06.024.

LaVigne, M., Grottoli, A.G., Palardy, J.E., Sherrell, R.M., 2016. Multi-colony calibrations of coral Ba/Ca with contemporaneous in situ seawater barium record. Geochim. Cosmochim. Acta 179, 203–216.

LaVigne, M., Hill, T.M., Spero, H.J., Guilderson, T.P., 2011. Bamboo coral Ba/Ca: Calibration of a new deep ocean refractory nutrient proxy. Earth Planet. Sci. Lett. 312, 506–515. https://doi.org/10.1016/j.epsl.2011.10.013.

Lea, D., Boyle, E., 1989. Barium content of benthic foraminifera controlled by bottom-water composition. Nature 338, 751–753. https://doi.org/10.1038/338751a0.

Lea, D.W., Boyle, E.A., 1993. Determination of carbonate-bound barium in foraminifera and corals by isotope dilution plasma-mass spectrometry. Chem. Geol. 103 (1–4), 73–84. https://doi.org/10.1016/0009-2541(93)90292-Q.

Lea, D.W., Spero, H., 1994. Assessing the reliability of paleochemical tracers: barium uptake in the shells of planktonic foraminifera. Paleoceanography 9 (3), 445–452. https://doi.org/10.1029/94PA00151.

Liu, Y., Li, X., Zeng, Z., Yu, H-Y., Huang, F., Felis, T., Shen, C-C., 2019. Annually-resolved coral skeletal $\delta^{138/134}$Ba records: a new proxy for oceanic Ba cycling. Geochim. Cosmochim. Acta 247, 27–39. https://doi.org/10.1016/j.gca.2018.12.022.

Mavromatis, V., Goetschl, K.E., Grengg, C., Konrad, F., Purgstaller, B., Dietzel, M., 2018. Barium partitioning in calcite and aragonite as a function of growth rate. Geochim. Cosmochim. Acta 237, 65–78. https://doi.org/10.1016/j.gca.2018.06.018.

Mavromatis, V., van Zuilen, K., Purgstaller, B., Baldermann, A., Nagler, T.F., Dietzel, M., 2016. Barium isotope fractionation during witherite $BaCO_3$. Geochim. Cosmochim. Acta 190, 72–84. https://doi.org/10.1016/j.gca.2016.06.024.

McCorkle, D.C., Martin, P.A., Lea, D.W., Klinkhammer, G.P., 1995. Evidence of a dissolution effect on benthic foraminiferal shell chemistry: δ^{13}C, Cd/Ca, Ba/Ca, and Sr/Ca results from the Ontong Java Plateau. Paleoceanography 10 (4), 699–714. https://doi.org/10.1029/95PA01427.

Mucci, A., Morse, J.W., 1983. The incorporation of Mg^{2+} and Sr^{2+} into calcite overgrowths: influences of growth rate and solution composition. Geochim. Cosmochim. Acta 47 (2), 217–233.

Prouty, N.G., Roark, E.B., Andrews, A.H., Robinson, L.F., Hill, T., Sherwood, O., Williams, B., Guilderson, T., Fallon, S., 2017. Age, growth rates, and paleoclimate studies in deep-sea corals of the United States. In: Hourigan, T.F., Etnoyer, P.J., Cairns, S.D. (Eds.), The State of Deep-Sea Coral and Sponge Ecosystems of the United States. NOAA Technical Memorandum NMFS-OHC-4, Silver Spring, MD. 22 p.

Roark, E.B., Guilderson, T.P., Flood-Page, S., Dunbar, R.B., Ingram, B.L., Fallon, S.J., McCulloch, M., 2005. Radiocarbon-based ages and growth rates of bamboo corals from the Gulf of Alaska. Geophys. Res. Lett. 32 (4). https://doi.org/10.1029/2004GL021919.

Saenger, C., Watkins, J.M., 2016. A refined method for calculating paleotemperatures from linear correlations in bamboo coral carbon and oxygen isotopes. Paleoceanography 31 (6), 789–799. https://doi.org/10.1002/2016PA002931.

Serrato Marks, G., LaVigne, M., Hill, T., Sauthoff, W., Guilderson, T., Roark, E., Dunbar, R., Horner, T.J., 2017. Reproducibility of Ba/Ca variations recorded by northeast Pacific bamboo corals. Paleoceanography 32 (9), 966–979. https://doi.org/10.1002/2017PA003178.

Sherwood, O.A., Edinger, E.N., 2009. Ages and growth rates of some deep-sea gorgonian and antipatharian corals of newfoundland and labrador. Can. J. Fish. Aquat. Sci. 66 (1), 142–152. https://doi.org/10.1139/F08-195.

Sherwood, O.A., Risk, M.J., 2007. Chapter twelve deep-sea corals: new insights to paleoceanography. Dev. Mar. Geol. 1, 491–522. https://doi.org/10.1016/S1572-5480(07)01017-2.

Sigman, D.M., Hain, M.P., Haug, G.H., 2010. The polar ocean and glacial cycles in atmospheric CO_2 concentration. Nature 466, 47–55. https://doi.org/10.1038/nature09149.

Sinclair, D.J., Williams, B., Allard, G., Ghaleb, B., Fallon, S., Ross, S., Risk, M., 2011. Reproducibility of trace element profiles in a specimen of the deep-water bamboo coral Keratoisis sp. Geochim. Cosmochim. Acta 75 (18), 5101–5121. https://doi.org/10.1016/j.gca.2011.05.012.

Spooner, P.T., Robinson, L.F., Hemsing, F., Morris, P., Stewart, J.A., 2018. Extended calibration of cold-water coral Ba/Ca using multiple genera and co-located measurements of dissolved barium concentration. Chem. Geol. 499, 100–110. https://doi.org/10.1016/j.chemgeo.2018.09.012.

Talley, L.D., 2008. Freshwater transport estimates and the global overturning circulation: shallow, deep and throughflow components. Prog. Oceanogr. 78 (4), 257–303.

Thresher, R.E., Fallon, S.J., Townsend, A.T., 2016. A “core-top” screen for trace element proxies of environmental conditions and growth rates in the calcite skeletons of bamboo corals (isididae). Geochim. Cosmochim. Acta 193, 75–99. https://doi.org/10.1016/j.gca.2016.07.033.

Thresher, R., Rintoul, S.R., Koslow, J.A., Weidman, C., Adkins, J., Proctor, C., 2004. Oceanic evidence of climate change in southern Australia over the last three centuries. Geophys. Res. Lett. 31 (7). https://doi.org/10.1029/2003GL018869.

Thresher, R.E., Wilson, N.C., MacRae, C.M., Neil, H., 2010. Temperature effects on the calcite skeletal composition of deep-water gorgonians (isididae). Geochim. Cosmochim. Acta 74 (16), 4655–4670. https://doi.org/10.1016/j.gca.2010.05.024.

Toggweiler, J.R., 1999. Variation of atmospheric CO_2 by ventilation of the ocean's deepest water. Paleoceanography 14 (5), 571–588. https://doi.org/10.1029/1999PA900033.

von Allmen, K., Böttcher, M.E., Samankassou, E., Nägler, T.F., 2010. Barium isotope fractionation in the global barium cycle: first evidence from barium minerals and precipitation experiments. Chem. Geol. 277 (1–2), 70–77. https://doi.org/10.1016/j.chemgeo.2010.07.011.

Wolgemuth, K., Broecker, W.S., 1970. Barium in sea water. Earth Planet. Sci. Lett. 8 (5), 372–378. https://doi.org/10.1016/0012-821X(70)90110-X.